

# Charged Higgs Boson Pairs at the LHC

Alexandre Alves<sup>1</sup> and Tilman Plehn<sup>2\*</sup>

<sup>1</sup>*Instituto de Física, Universidade de São Paulo, São Paulo, Brasil and*

<sup>2</sup>*Max Planck Institute for Physics, Munich, Germany*

We compute the cross section for pair production of charged Higgs bosons at the LHC and compare the three production mechanisms. The bottom-parton scattering process is computed to NLO, and the validity of the bottom-parton approach is established in detail. The light-flavor Drell-Yan cross section is evaluated at NLO as well. The gluon fusion process through a one-loop amplitude is then compared with these two results. We show how a complete sample of events could look, in terms of total cross sections and distributions of the heavy final states.

## I. SETTING THE STAGE

Understanding electroweak symmetry breaking is arguably the biggest challenge in particle physics, and we are confident that we will solve it at the LHC. In the Standard Model, a single Higgs doublet gives mass to the up-type and down-type quarks and also manifests itself as one scalar Higgs boson. Electroweak precision data indicates that this Higgs boson is light [1]. In the supersymmetric extension of the Standard Model we need two Higgs doublets to give mass to the up-type and down-type quarks and to cancel anomalies of the fermionic partners of the Higgs bosons. The particle content of a two-Higgs doublet model (2HDM) consists of two scalars, a pseudo-scalar and a charged Higgs boson. It has been shown that the LHC is guaranteed to find one supersymmetric Higgs boson in the weak boson fusion production process with subsequent decay to tau leptons [2, 3]. However, if we want to test a supersymmetric Higgs sector the charged Higgs boson becomes crucial. While there are many ways to add scalars to the Standard Model spectrum and allow them to mix with the Higgs boson, for example radions [4], a charged Higgs boson with all the appropriate couplings as in the 2HDM is much harder to fake.

### A. Charged Higgs Bosons at the LHC

Over the years, there have been many studies of charged Higgs bosons at the LHC. The dominant production processes are in association with a top quark [5, 6, 7, 8], in association with a  $W$  boson [9, 10], and charged Higgs pair production [11, 12, 13, 14, 15, 16, 17]. The most promising decay channels are (depending on the charged Higgs mass)  $\tau\bar{\nu}$  [18, 19, 20],  $b\bar{t}$  [21, 22, 23], and  $Wh^0$  [24]. According to studies by ATLAS [19] and CMS [20], the process  $pp \rightarrow tH^- \rightarrow t(\tau\bar{\nu})$  is currently the most promising combination, in particular for large values of  $\tan\beta$ . The reason is that the Yukawa coupling of the charged Higgs boson to quarks includes a term proportional to  $m_b \tan\beta$ , which means that the  $tH$  production cross section is enhanced by a factor  $\tan^2\beta$ . Unfortunately, the same studies indicate that for  $m_H > m_t$  the  $tH$  production channel fails for  $\tan\beta \lesssim 10$  because of the reduced production rate.

Pair production of charged Higgs bosons is particularly interesting because three different production processes contribute to the same final state: the usual Drell-Yan production process  $q\bar{q} \rightarrow H^+H^-$  through an  $s$ -channel  $Z$  or a photon [11], the loop-induced gluon fusion process  $gg \rightarrow H^+H^-$  [12, 13, 14], and bottom-parton scattering  $b\bar{b} \rightarrow H^+H^-$ . The latter two are enhanced as  $\sigma \propto \tan^4\beta$  for large values of  $\tan\beta$ , which can compensate for the loop factor suppression or the small bottom parton density. The idea of this paper is twofold. First, in a detailed study (including a next-to-leading order (NLO) calculation of the total cross section) of the process  $b\bar{b} \rightarrow H^+H^-$ , we establish a reliable prediction for its rate. Second, we show how the different production cross sections can be added and how they contribute in the different areas of 2HDM parameter space. In a brief addendum we will estimate the supersymmetric QCD corrections to the process  $b\bar{b} \rightarrow H^+H^-$  and test the reliability of the approximation for the complete set of supersymmetric diagrams by the leading (resummed)  $\tan\beta$  contributions.

### B. Bottom Parton Picture

The  $\tan\beta$  enhancement of the charged Higgs Yukawa coupling, which consists of one term proportional to  $m_b \tan\beta$  and another one proportional to  $m_t \cot\beta$ , immediately directs us to consider processes with bottom quarks in the initial state.

---

\* Heisenberg Fellow.

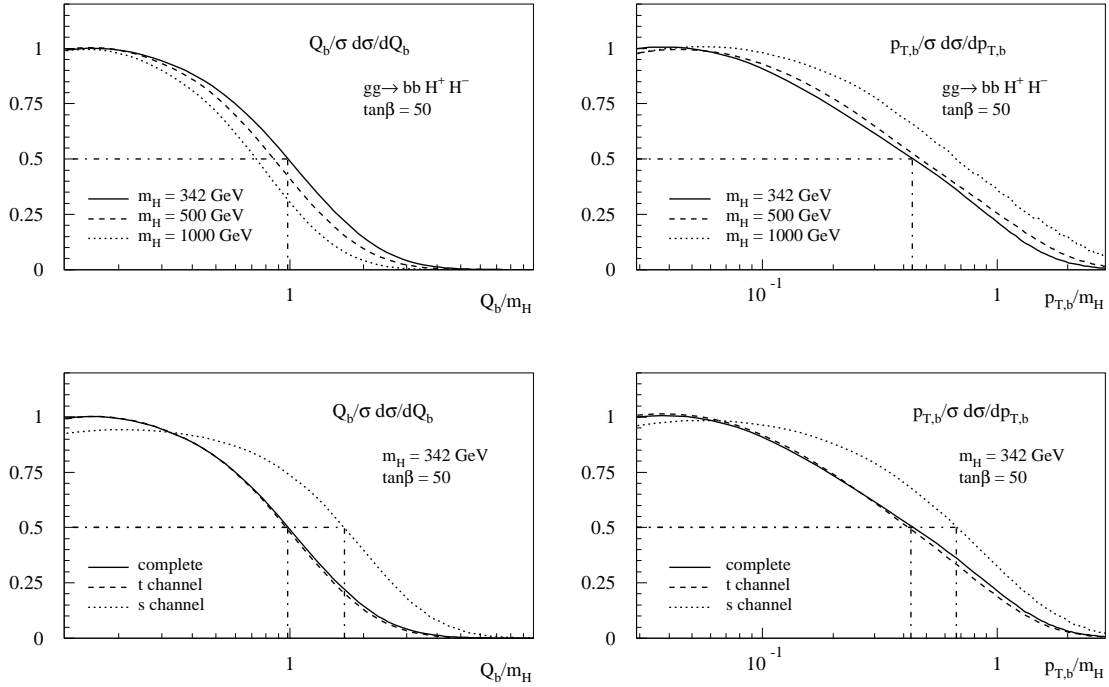


Figure 1: The dependence of the bottom-exclusive process  $gg \rightarrow \bar{b}bH^+H^-$  on the bottom virtuality and transverse momentum. The upper set of figures show the variation with charged Higgs mass, while the lower figures show the distributions for the different contributing subprocesses, namely a  $t$ -channel top quark and an  $s$ -channel  $Z$  boson and photon. The  $s$ -channel Higgs contributions are heavily suppressed for this choice of parameters. We see that the shoulders of the  $p_{T,b}$  distributions extend to values around  $m_H/2$  or  $M/4$  if the mass of the final state is identified with  $M \equiv 2m_H$  [6, 7].

Conceptually, this leads to the proper description of bottom partons. Lacking a measurement of bottom quarks in the proton, we calculate a bottom parton density from the gluon density, with gluons splitting into a bottom quark pair. Because the bottom mass is much larger than  $\Lambda_{\text{QCD}}$ , this splitting can be described perturbatively. It involves a large logarithm, which can be resummed using DGLAP evolution [25].

We illustrate the bottom-parton approach using the process  $bg \rightarrow tH^-$  [6, 7, 26], but the arguments given in this section are completely general. First, we compute the total cross section for the gluon-induced process (e.g.  $gg \rightarrow \bar{b}tH^-$ ), integrating over the final state bottom quark. This class of processes with explicit gluon splitting into bottom quarks, and with a bottom jet in the final state, we refer to as bottom-exclusive. In the limit of vanishing  $m_b$ , the differential cross section with respect to the transverse momentum of the bottom quark will diverge like  $d\sigma/dp_{T,b} \sim 1/p_{T,b}$ . The cross section after integrating over the phase space of the outgoing bottom quark will (again for vanishing  $m_b$ ) be approximately proportional to  $\log(p_{T,b}^{\text{max}}/p_{T,b}^{\text{min}})$ . In the presence of a finite bottom mass,  $m_b$  regularizes the cross section and yields a dependence  $\log(p_{T,b}^{\text{max}}/m_b)$ . If the upper integration boundary is given by some hard scale in the process, for example the masses of some heavy final state particles  $M = m_H + m_t \gg m_b$ , the total cross section after integrating over the bottom jet will be proportional to a large logarithm  $\log M/m_b$ . This logarithm can be resummed: switching from the bottom-exclusive process  $gg \rightarrow \bar{b}tH^-$  to the bottom-parton induced (bottom-inclusive) process  $bg \rightarrow tH^-$  does precisely that. From the above argument it is obvious that the bottom parton density as a function of the bottom factorization scale grows roughly like the leading logarithmic contribution  $\log \mu_{F,b}$ .

Historically, bottom-parton induced processes overestimated the total cross section if compared to their exclusive counterpart. The reason was that the bottom-parton description introduces a new parameter, namely the factorization scale of the bottom parton. It corresponds to the maximum transverse momentum of the final state bottom quark which is included in the bottom parton density. Since the bottom density is currently perturbatively calculated we can estimate the value of  $\mu_{F,b}$ , because it is implicitly part of the definition of the bottom partons: it is the maximum value of  $p_{T,b}$  in the bottom-exclusive process (again e.g.  $gg \rightarrow \bar{b}tH^-$ ) for which the differential cross section  $d\sigma/dp_{T,b}$  behaves like  $1/p_{T,b}$  and can therefore contribute to the bottom parton density — or in terms of the discussion in the previous paragraph:  $\mu_{F,b} \equiv p_{T,b}^{\text{max}}$ . Following a naive dimensional argument and identifying  $\mu_{F,b} = M$  implicitly assumes that the asymptotic behavior of the bottom-exclusive process extends to  $p_{T,b}^{\text{max}} = M$ . If for some reason  $p_{T,b}^{\text{max}} < M$  this will automatically lead to an overestimate of the total bottom-inclusive cross section.

In previous work [6, 7, 26] we showed that indeed at the LHC it is more appropriate to choose a smaller scale,  $\mu_{F,b} \equiv p_{T,b}^{\text{max}} \sim$

$M/4$ , where  $M$  is the hard scale in the process, *i.e.* the mass of the heavy states  $M_X$  in the process  $gg \rightarrow \bar{b}X$  or  $gg \rightarrow \bar{b}\bar{b}X$ . This scale choice can be derived in general from the kinematics of the exclusive process at the LHC [26]. Higher order calculations of the processes  $b\bar{b} \rightarrow H$  [27] and  $bg \rightarrow bH$  [28] have shown that this choice of factorization scale is supported by the stability of the perturbative series in  $\alpha_s$ . The perturbative behavior of the total cross section  $bg \rightarrow tH^-$  also confirms this choice of scales. Moreover, a comparison between the NLO results for the exclusive process  $gg \rightarrow \bar{b}\bar{b}H$  [29] and the one- or two-bottom inclusive processes  $bg \rightarrow bH$  and  $b\bar{b} \rightarrow H$  showed that the different results are now in good agreement [28]. Note that the different cross sections should not agree perfectly, as they include contributions at different orders in perturbation theory. Because they differ mostly by the fact that the bottom-parton induced processes resum the logarithm  $\log(p_{T,b}^{\max}/m_b)$ , the agreement should be better for small final state masses, in our case small  $m_H$ . On the other hand, they should agree within their perturbative error bands, because we know the difference between the calculations and we can estimate their respective theoretical errors.

Going beyond total cross sections, we showed in Ref. [7] that for the process  $bg \rightarrow tH^-$ , the distributions of the heavy final state particles are not affected by the approximations of the bottom parton picture, namely the assumption that the incoming bottom quarks are massless and that they are collinear. These issues will be addressed for  $b\bar{b} \rightarrow H^+H^-$  in section III.

Before we analyze bottom-induced charged Higgs pair production, we perform a consistency check. Based on general kinematical arguments, it was shown that for LHC production processes the bottom factorization scale should be chosen around  $M/4 = m_H/2$ . We repeat the numerical analyses of Refs. [6, 7, 28] and show the results on which this argument is based in Fig. 1. The two left panels show the intermediate bottom virtuality, the right pair show the transverse momentum of the intermediate or final state bottom. In accordance with earlier results we see that the shoulder limiting the  $1/Q_b$  or  $1/p_{T,b}$  behavior for large momentum transfer sits at smaller values for the transverse momentum than for the virtuality. For different charged Higgs masses both shoulders scale with the mass, which is equivalent to the claim that the bottom factorization scale has to be proportional to the hard scale  $\mu_{F,b} \propto M = 2m_H$ . The smaller maximum values of  $Q_b$  and  $p_{T,b}$  for larger values of the charged Higgs mass is indicative of the limited phase space at the LHC. The value for  $p_{T,b}^{\max}$ , up to which we can observe something like a  $1/p_{T,b}$  behavior, is clearly smaller than  $M = 2m_H$  and in agreement with the general estimate  $\mu_{F,b} \sim M/4 = m_H/2$ . Also in Fig. 1 we see that the shoulder for the  $s$ -channel process extends to larger values of  $Q_b$  and  $p_{T,b}$  by about a factor of 1.5. This can be understood from the approximate determination of the factorization scale in Ref. [26]: the position of the shoulders in the  $Q_b$  and the  $p_{T,b}$  curves can be approximately computed relying only on the parton  $x$  behavior of the gluon density. However, the results  $Q_b^{\max} \sim M/2$  and  $p_{T,b}^{\max} \sim M/4$  assume that the heavy final state is produced at threshold. The difference between the  $s$ -channel and  $t$ -channel processes is that  $t$ -channel Higgs pair production can proceed through an  $S$  wave, which cross section increases proportional to the Higgs velocity  $\beta$  [41] at threshold, while the  $s$ -channel process increases like  $\beta^3$  and therefore shows a delayed onset. The  $s$ -channel process is strongly suppressed at threshold and produces the bulk of the Higgs pairs at a larger partonic center-of-mass energy (we show the corresponding  $p_{T,H}$  distributions in sections II and IV). Thus, for the  $s$ -channel process, the typical final state invariant mass is larger, which means effectively  $M > 2m_H$ . This is what we observe for the gauge boson exchange process in Fig. 1. We also notice that the determination of the bottom factorization scale has a theoretical error, because we have to approximate the physical curves with a box-shaped object. Effects like threshold suppression of the  $s$ -channel diagrams are covered by the theoretical error, and we discuss the different scale variations in detail in section II.

### Organization of the Paper and Conventions

The paper is organized as follows: in this section we reviewed the status of charged Higgs searches at the LHC and the status of the bottom-parton approach. In section II we compute the bottom-parton induced cross section to NLO. We show how the description is perturbatively stable with respect to QCD corrections. In section III we use the NLO predictions for the distributions of the heavy final states to prove the validity of the bottom-parton approach. The results from these two sections allow us to quantitatively compare the different production processes for charged Higgs pairs at the LHC in section IV. This comparison covers total rates as well as differential cross sections. As an addendum we compute the full SUSY-QCD corrections to the bottom-parton scattering process in section V.

Before we proceed with the discussion of the results we briefly give all conventions used for our calculations. All bottom-parton induced cross sections are computed with zero bottom mass. When we check our results using final state bottom quarks we use the on-shell mass  $m_b = 4.6$  GeV, or for testing purposes a second value 0.46 GeV. The top quark mass is always chosen as  $m_t = 178$  GeV. In contrast, the bottom and top Yukawa couplings are defined in the  $\overline{\text{MS}}$  scheme, *i.e.* numerically we use  $m_b(\mu_R)$  and  $m_t(\mu_R)$ . Unless explicitly mentioned we use the renormalization scale  $\mu_R = m_H$  and the bottom factorization scale  $\mu_{F,b} = m_H/2$ . The parton densities are CTEQ6 [31], consistently chosen to be the LO or NLO sets L1 or M;  $\alpha_s$  is also calculated at equivalent order.

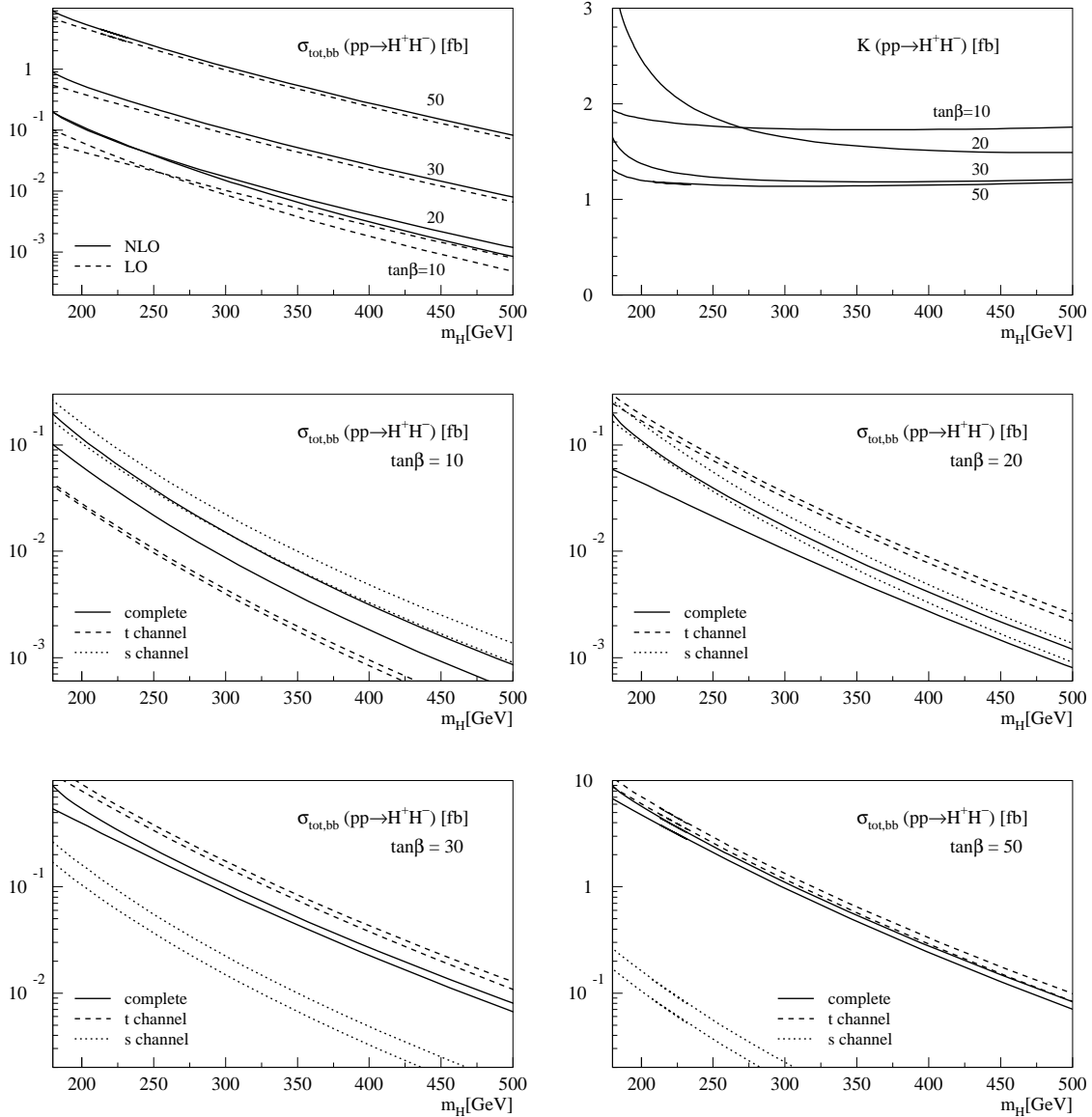


Figure 2: LO and NLO total cross section for the process  $b\bar{b} \rightarrow H^+H^-$  at the LHC. The  $K$  factor is defined consistently as  $\sigma_{\text{NLO}}/\sigma_{\text{LO}}$ . The parameters in the 2HDM Higgs sector are chosen consistently for each value of  $\tan\beta$  and charged Higgs mass  $m_H$ . In the lower two rows the contributions from  $s$ -channel Higgs and  $\gamma, Z$  exchange and  $t$ -channel top quark exchange are shown. In those figures the NLO curve is always the upper one in each pair.

## II. BOTTOM-INDUCED PRODUCTION PROCESS

Before we can discuss the different charged Higgs pair production processes at the LHC (in section IV), we have to find a way to reliably predict the bottom-induced production rate  $b\bar{b} \rightarrow H^+H^-$ . This shortcoming was noticed in an earlier paper [13], and with the recent progress in understanding bottom-parton induced processes we can now fill this gap. The key ingredient for the correct evaluation of production processes of the kind  $b\bar{b} \rightarrow H^+H^-$  is the choice of bottom parton factorization scale, which we reviewed in detail in section IB. Next, we will compute the NLO corrections (for now in the 2HDM, *i.e.* without gluino contributions, which are added in section V).

We calculate the  $\mathcal{O}(\alpha_s)$  corrections to the process  $pp/b\bar{b} \rightarrow H^+H^- + X$  following two different approaches. First, we use a one-cutoff technique to calculate the total cross sections. These results will be made publicly available as part of an extension to the Prospino2 package [30]. This approach has the advantage of being numerically fast and reliable. In a second step we repeat the calculation with two cutoffs for the soft ( $\delta_s = 10^{-4}$ ) and collinear ( $\delta_c = \delta_s/100$ ) divergences [32]. This allows us

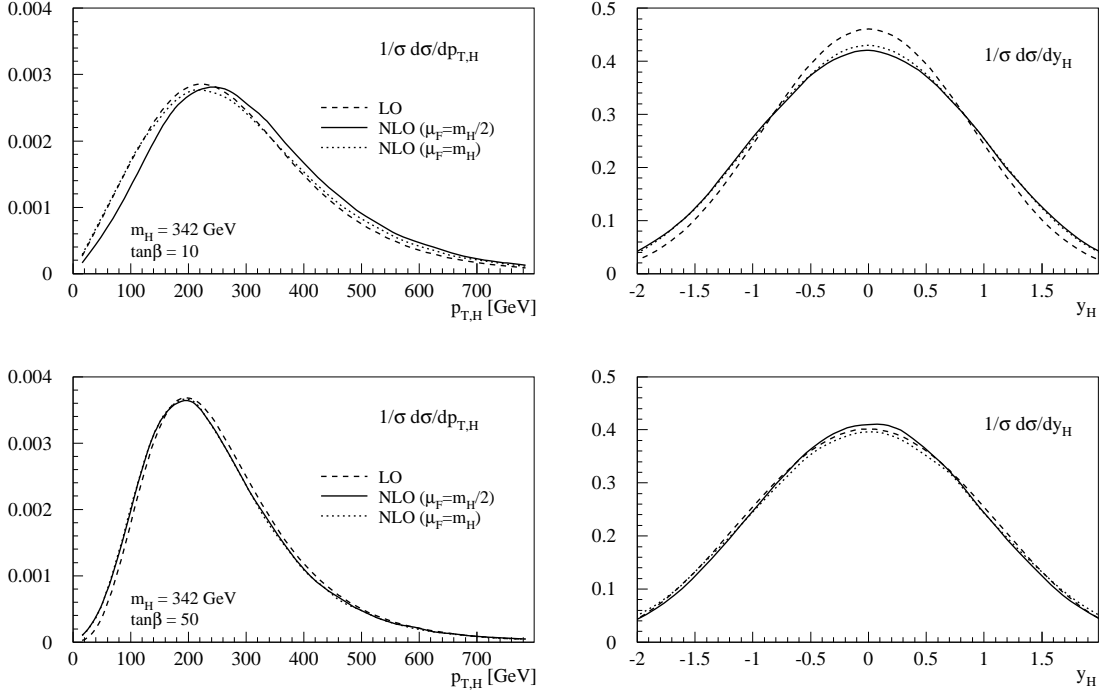


Figure 3: The rapidity and transverse momentum distributions at LO and NLO. The results are shown for two different values of  $\tan\beta$ , so illustrate the behavior of the  $s$ -channel and the  $t$ -channel diagrams. We include a set of NLO curves for the factorization scale  $\mu_F = 2\mu_F^0 = m_H$  to illustrate the remaining theoretical uncertainty.

to calculate distributions for the heavy final state particles. These distributions are a crucial check of the validity of the bottom-parton approximation, which we use to improve the prediction of the total cross section. Moreover, we will be able to compare the differential cross sections for the different charged Higgs pair production mechanisms in section IV.

**NLO corrections:** We present the results of our NLO calculation in Fig. 2. The total cross sections are plotted as a function of the charged Higgs mass for four different values of  $\tan\beta$ . The 2HDM parameters are chosen consistently [33]. Before discussing the higher-order corrections we note that indeed the leading order (LO) cross section increases like  $\tan^4\beta$  for large values of  $\tan\beta$ . The  $K$  factor in the second panel is defined as  $\sigma_{\text{NLO}}/\sigma_{\text{LO}}$ . The size of the NLO correction is strongly dependent on the Higgs mass and on the value of  $\tan\beta$ . To understand this we separate the three different contributions to the production rate.

The bottom-induced Drell-Yan contribution proceeds through an  $s$ -channel photon or  $Z$  boson. The coupling to the photon is independent of  $\tan\beta$  and the dependence of the  $Z$  coupling is small for large enough values of the pseudoscalar and charged Higgs masses (the decoupling limit). The NLO corrections for the bottom-induced Drell-Yan process vary around  $K = 1.60 \cdots 1.55$  for Higgs masses from 160 GeV to 500 GeV. This correction is somewhat larger than for the light-flavor Drell-Yan process, which is due to the  $x$  dependence of the bottom parton densities and can also be observed in the perturbative behavior of the Standard Model  $b\bar{b} \rightarrow H$  process [27].

A second set of  $s$ -channel production processes is made possible by the incoming bottom quarks and their finite Yukawa coupling: we can couple the charged Higgs pair to  $s$ -channel neutral CP-even Higgs bosons  $h^0, H^0$ . CP-odd pseudoscalar exchange is forbidden by the CP symmetry of the final state. The Higgs self-couplings  $h^0 H^+ H^-$  and  $H^0 H^+ H^-$  are strongly dependent on the Higgs sector [12] parameters, but the relative size of the Higgs contribution compared to the Drell-Yan process is basically negligible; the suppression varies from  $10^{-2}$  for small Higgs masses below 200 GeV to  $10^{-3}$  for Higgs masses around 500 GeV. While it is possible that there are regions of 2HDM parameter space where this hierarchy is less pronounced, the impact of the  $s$ -channel Higgs exchange is small for our analysis. We note, however, that the NLO corrections to the  $s$ -channel Higgs exchange are smaller than for the Drell-Yan process, namely  $K = 1.15 \cdots 1.20$  (for charged Higgs masses from 160 GeV to 500 GeV). This is in part an effect of the  $\overline{\text{MS}}$  renormalization of the bottom Yukawa coupling. The combination of the two  $s$ -channel processes receives a fairly constant NLO correction, from  $K = 1.58$  for small Higgs masses and  $\tan\beta = 10$  to  $K = 1.55$  for large values of  $\tan\beta$  or large Higgs masses.

For the total rate the  $s$ -channel production processes compete with  $t$ -channel top quark exchange. The  $btH^+$  coupling consists of two contributions,  $y_b \tan\beta$  and  $y_t \cot\beta$ . Over the entire parameter space  $\tan\beta > 10$ , the  $y_b^4$  contribution dominates over

the  $y_t^4$  contribution by at least one order of magnitude. We note that because of the different running of the bottom and top Yukawa couplings the  $K$  factor of the  $y_b^4$  contribution is considerably smaller than for the  $y_t^4$  contribution [6]. This leads to a  $\tan\beta$  dependence of the NLO corrections to the  $t$ -channel process. For small Higgs masses the size of the correction varies as  $K = 1.06 \cdots 1.36$  (for  $\tan\beta = 10$  to 50). For larger values of the Higgs masses (and thereby the renormalization scale) the behavior of  $K$  becomes flat.

Combining the  $s$ -channel and  $t$ -channel contributions, we see that they interfere destructively. For small Higgs masses the LO rates are almost identical in size for  $\tan\beta \sim 20$ . Because the two classes of diagrams have very different NLO corrections this leads to huge relative QCD corrections to the total rate. We observe this in Fig. 2, where the  $K$  factors are fairly constant for the  $s$ -channel dominated regime  $\tan\beta \lesssim 10$ , and for the  $t$ -channel dominated regime  $\tan\beta \gtrsim 30$ . The curve for  $\tan\beta = 30$  shows a small remaining increase only for very small Higgs masses. The slight difference between the large  $m_H$  behavior of the  $\tan\beta = 30$  and  $\tan\beta = 50$  curves is also due to the interference between the  $s$ - and  $t$ -channel subprocesses.

We emphasize that in this paper we show results only for large charged Higgs masses  $m_H > m_t$ . For small Higgs masses there is a technical complication, because the production process  $bg \rightarrow tH^-$  and its charge conjugate will be part of the NLO corrections. We subtract the corresponding divergence consistently in the small width approximation, which is also used in Refs. [7, 30, 34]. The public computer code in the extension to Prospino2 will, however, include this region of parameter space. Phenomenologically it is less interesting, because charged Higgs bosons will be produced in large numbers in anomalous top quark decays. Matching with the off-shell process  $bg \rightarrow tH^-$  is studied in detail in Ref. [7].

**Distributions:** The effect of NLO corrections on the distributions of the heavy final state Higgs bosons is shown in Fig. 3. The case  $\tan\beta = 50$  corresponds to the parameter point SPS4 [35], and the parameter choice  $\tan\beta = 10$  is the same in all parameters except for  $\tan\beta$ . According to Fig. 2,  $t$ -channel top quark exchange is effectively switched off this way. All that is left is  $s$ -channel gauge boson exchange. For  $\tan\beta = 50$ , the rate is completely dominated by  $t$ -channel top exchange: the relative size of the two contributions,  $\sigma_{s,\text{only}}/\sigma_{t,\text{only}}$ , varies from 2.0% to 1.0% at LO and from 2.5% to 1.5% at NLO (with a charged Higgs mass between 200 GeV and 500 GeV). While the shift in this fraction is sizable, as we would expect from the different  $K$  factors described above, any distribution for  $\tan\beta = 50$  will be completely independent of the  $s$ -channel contributions. Similar to higher order corrections to supersymmetric particle production [30], we indeed see that a constant  $K$  factor in the  $(p_{T,H} - y_H)$  plane is a reasonable approximation within any error estimate.

The situation is slightly different for  $\tan\beta = 10$ . Here the peak in the  $p_{T,H}$  distribution shifts by 20 GeV when we switch to the slightly harder NLO description. The interference between the  $s$  channel and the  $t$  channel subprocesses plays no role —  $\sigma_{t,\text{only}}/\sigma_{s,\text{only}}$  decreases from typically 0.25 at LO to NLO values around 0.18, which we checked is not sufficient to impact the distributions visibly. Instead, the shift towards a slightly harder spectrum is a result of the three-particle phase space at NLO. The extra jet balances the slightly harder charged Higgs bosons in the final state. The same effect actually appears for  $\tan\beta = 50$ , but it is less pronounced. To estimate how the shift in the  $p_{T,H}$  distribution compares with the theoretical uncertainty, and to understand the difference in the size of the shift between  $s$ -channel and  $t$ -channel diagrams, we change the bottom factorization scale to twice its usual value:  $\mu_F = m_H$ . From section IB we know that this will make the  $s$ -channel ( $P$ -wave) subprocess more similar to  $t$ -channel ( $S$ -wave) top quark exchange. Indeed, in Fig. 3 we see that the LO curve shows no visible effect, and that the NLO and the LO distributions are now almost identical.

As we pointed out in section IB the determination of the bottom factorization scale shows an inherent theoretical error, because it is not possible to tell where exactly the asymptotic behavior of the bottom-exclusive processes is no longer valid. The observed scale-dependent shift between the LO and NLO distributions reflects this remaining theoretical uncertainty, and shows that it is perturbatively under control.

**Scale dependence:** Even though we have argued before that the bottom factorization scale should be chosen around  $m_H/2$ , the renormalization and factorization scales are nevertheless free parameters introduced by the perturbative expansion of the hadronic production cross sections. The bottom factorization scale plays a special role, because it is not actually extracted from data. Instead, it is calculated from the measured gluon density in a perturbative regime. However, while we can claim what the (roughly) appropriate values for  $\mu_{F,b}$  should be, it is also obvious from Fig. 1 that a serious theoretical error margin should be assigned to the determination of the appropriate scale. We therefore proceed to check the factorization and renormalization scale dependence of the cross section  $pp \rightarrow H^+H^-$  at LO and NLO. Because the scales are artifacts of perturbation theory, we expect the scale dependence to be a measure of the theoretical error on the total cross section, and we expect it to flatten after we include the NLO contributions.

The scale dependences of the LO and NLO cross sections are shown in Fig. 4. For the two dimensional plots both scales are varied up to factors 1/10 and 10, respectively, around their central values  $\mu_F^0 = m_H/2$  and  $\mu_R^0 = m_H$ . The central value of the factorization scale was motivated in section IB, and the central value of the renormalization scale is motivated by the production of heavy supersymmetric particles at the LHC [30] and by the production of Higgs bosons from bottom-parton initial states [6, 7, 27]. Note that the renormalization scale covers the running top and bottom Yukawa couplings at LO, whereas the strong coupling  $\alpha_s$  only enters at NLO.

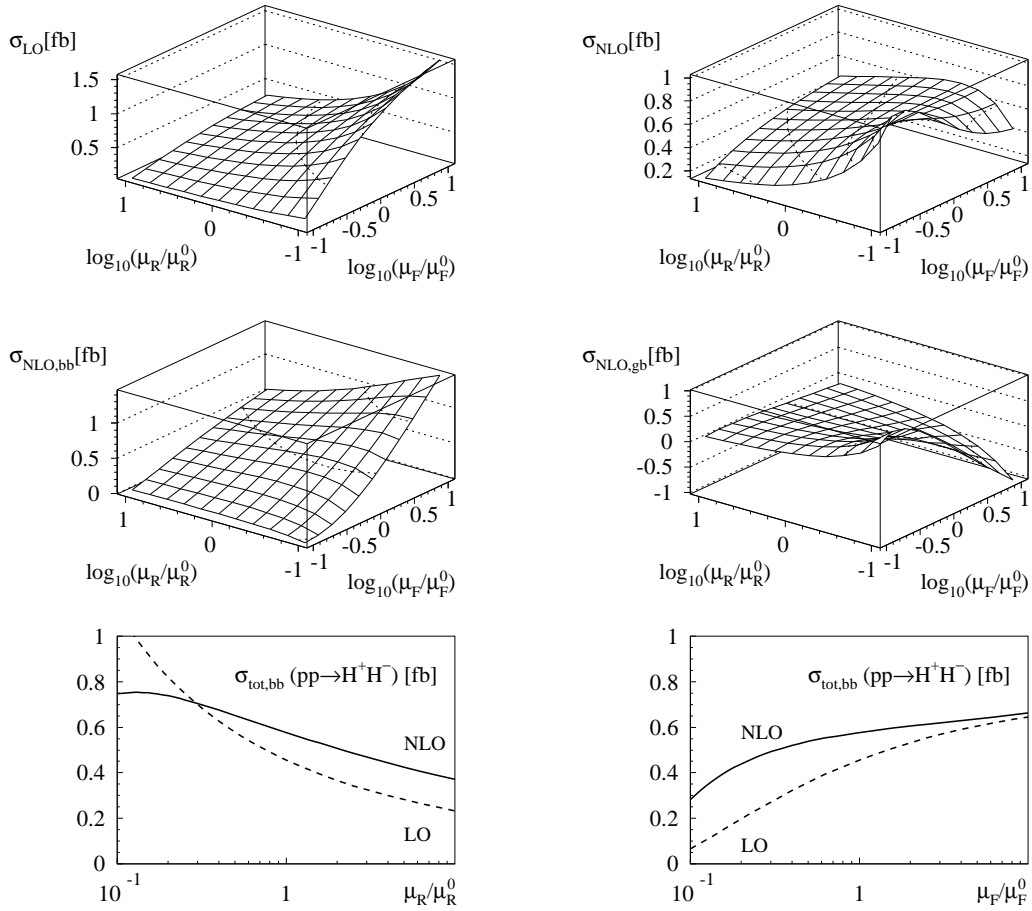


Figure 4: Factorization and renormalization scale dependence of the total cross section. The scales are varied around the central values  $\mu_F^0 = m_H/2$  and  $\mu_R^0 = m_H$ . In the second row the contributions to the NLO rate are separated by their different initial state. In the third row the scale, which is not varied, is fixed to its respective value  $\mu^0$ . The LO curves are the dashed ones and the NLO curves are the solid lines. For the charged Higgs mass we use our central parameter point SPS4 with  $\tan \beta = 50$  and  $m_H = 342$  GeV.

From the two-dimensional behavior shown in Fig. 4, we see that the NLO rate has a considerably flatter scale dependence than its LO counterpart. There is, however, one exception to this rule: for very small  $\mu_F$  and very small  $\mu_R$  the perturbative expansion of the process  $b\bar{b} \rightarrow H^+H^-$  becomes unstable. This is the regime where the bottom-parton description breaks down: a small bottom factorization scale means that hardly any phase space of the gluon splitting in the bottom-exclusive process is resummed and very little of the bottom-exclusive production rate is included in the bottom parton density. This means that the  $bg$ -induced process which contributes to the NLO rate will dominate over the  $b\bar{b}$ -induced LO process. This effect becomes more pronounced if the perturbative expansion parameter which suppressed the  $bg$ -induced channel as compared the  $b\bar{b}$ -induced Born process is large, *i.e.* for a small renormalization scale which increases the value of  $\alpha_s(\mu_R)$ . The same feature can be seen in the associated production of a charged Higgs with a top quark [7].

If we stay away from this (and unphysical) scale choice, we can attempt to estimate the theoretical error of the LO and NLO total cross sections for  $pp/b\bar{b} \rightarrow H^+H^- + X$ . A reasonable range of scales could be a band from  $\mu^0/3$  to  $3\mu^0$  around the central values. First, we see that the LO and NLO error bands for both scales would overlap in Fig 4. This is not crucial, but it is certainly a welcome feature, which indicates that there are no large constant terms entering the cross section calculation at the NLO level. Moreover, we see that the factorization scale dependence covers a little less than a 20% error band, and the renormalization scale points to an error slightly above 10%. Even though the two scale dependences cancel each other if we identify  $\mu_R/\mu_R^0 \sim \mu_F/\mu_F^0$  we prefer to conservatively estimate the overall error by adding the two errors in square. This leads us to an estimate of the theoretical error (due to higher order corrections) for the NLO total cross section prediction of around 25%. We emphasize that this estimate cannot be a precise error band with a statistical meaning, as for example statistical or systematic experimental errors are. The range of scales we choose to cover is not fixed by first principles, and it is by no means guaranteed that no large finite terms come in at the NNLO level. However, we know that we have resummed the leading large

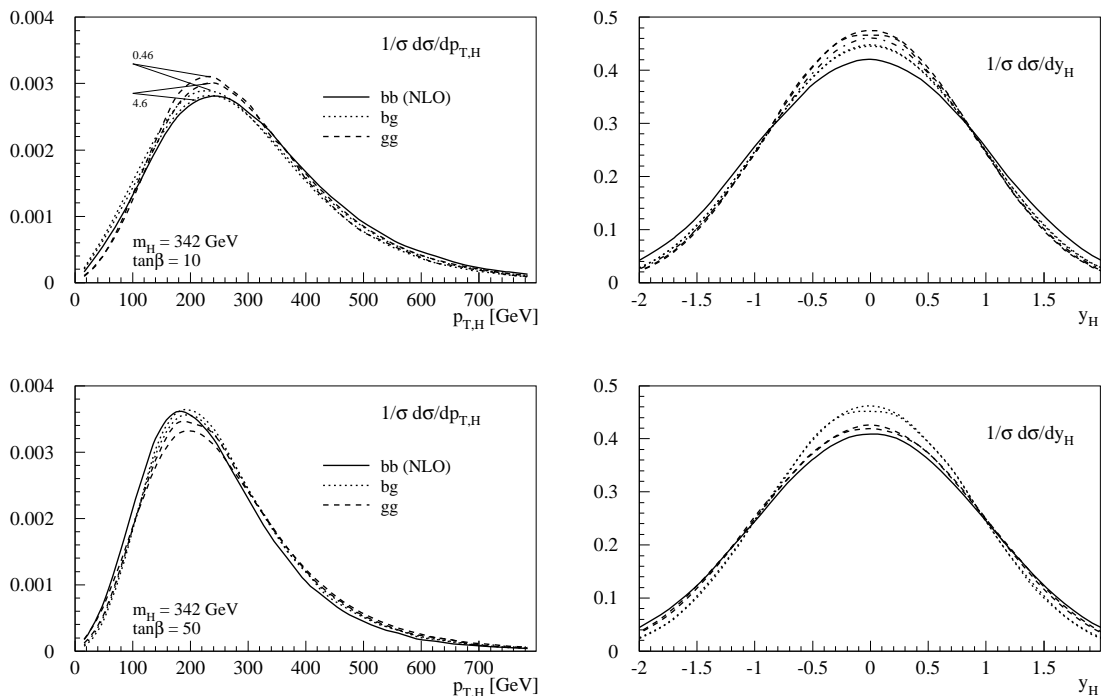


Figure 5: The rapidity and transverse momentum distributions of the final state charged Higgs boson for different processes. The two-bottom and one-bottom exclusive results (with the initial states  $gg$  and  $bg$ ) are given for the physical mass  $m_b = 4.6$  GeV and for a hypothetical value of  $0.46$  GeV. The NLO results for the  $bb$ -initiated process is shown for massless bottom quarks.

logarithms into the bottom parton densities, and we see a well behaved perturbative behavior going from the LO to the NLO cross section calculation.

### III. BOTTOM PARTON APPROXIMATION

The bottom-parton approach which we use to compute the double-bottom inclusive process  $b\bar{b} \rightarrow H^+H^-$  resums large logarithms and improves the prediction of the bottom-inclusive cross sections, but it also implicitly makes two approximations. One is that incoming bottoms are massless, the other one is that the bottom jets over which we integrate are collinear. For total cross sections these approximations are well founded: bottom mass effects are suppressed by powers of  $m_b/m_H$ , so they are well below any errors we quote on the NLO total cross section calculation. The kinematical configuration of the final state does not enter the computation of the total cross section, which means that we do not expect any non-negligible finite- $p_{T,b}$  effects for the total cross section calculation using bottom partons.

In section IB we showed that the bottom-parton approach works well for total cross sections. In some sense this is by construction, because we estimate the value of the only new parameter, the bottom factorization scale, such that the total cross section prediction is consistent with the definition of the bottom parton densities as they are computed from the bottom-exclusive process. The only serious test of the bottom-parton approach is the check that our estimate of the factorization scale indeed predicts  $\mu_{F,b} \propto M$ , where  $M$  is the hard scale in the process, usually chosen as the sum of final state masses. Differential cross sections, in contrast, are a non-trivial check of our approach. Phenomenologically it is crucial that the distributions of the heavy final states are not significantly affected by the two approximations mentioned above (here, significantly means with a larger effect than the perturbative error of the NLO calculation, which we estimated to be around 25% for the total cross section).

Massless bottom quark approximation: The first approximation we have to check is the assumption that the bottom partons and bottom jets involved are assumed to be massless. This is easy to estimate, because we can compute the one-bottom or two-bottom exclusive processes at tree level with different bottom masses. There is a technical complication in the one-bottom exclusive processes  $bg \rightarrow bH^+H^-$ , where we have to choose the incoming bottom as massless and the outgoing bottom as massive. Because of SU(3) gauge invariance we cannot couple a massless bottom and a massive bottom to a gluon. However, in our  $s$  and  $t$ -channel diagrams we are not sensitive to U(1) or SU(2) gauge invariance, so we can switch from massless incoming bottoms to massive outgoing bottoms at the  $bbZ$  and  $bb\gamma$  vertices.



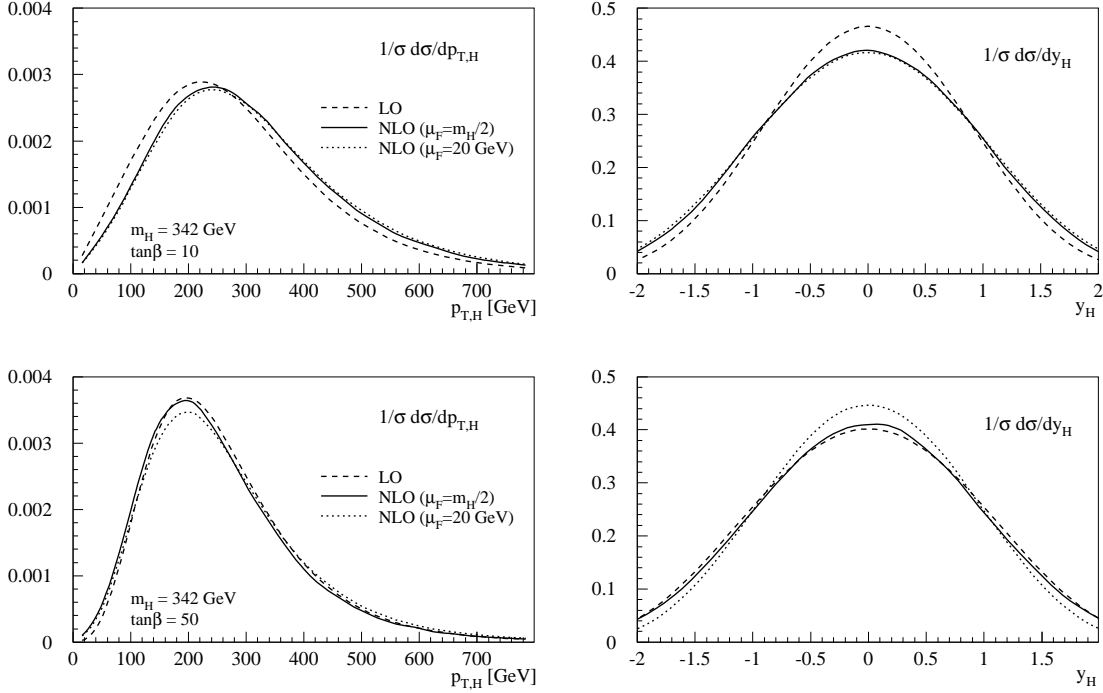


Figure 6: The rapidity and transverse momentum distributions for the final state charged Higgs boson for different choices of the factorization scale. The small scale choice  $\mu_{F,b} = 20$  GeV interpolates into the region where the formally-NLO subprocess  $bg \rightarrow bH^+H^-$  dominates the NLO rate.

We compute all distributions for the physical on-shell mass  $m_b = 4.6$  GeV and for a hypothetical 0.46 GeV. Apart from the NLO predictions for the bottom-inclusive process  $b\bar{b} \rightarrow H^+H^-$ , the normalized distributions for the rapidity and the transverse momentum of the final state Higgs bosons are computed for the processes  $gg \rightarrow b\bar{b}H^+H^-$  and  $bg \rightarrow bH^+H^-$ . These five curves are shown in Fig. 5. Because the  $s$ -channel neutral Higgs bosons do not contribute visibly, one can think of the different values of  $\tan\beta$  as a rescaling of the independent Yukawa couplings; the parameter choice  $\tan\beta = 10$  switches off  $t$ -channel top quark exchange and leaves us with  $s$ -channel gauge boson exchange.

In Fig. 5 we see that the bands defined by varying the bottom mass for a given process are considerably smaller than the difference between the different initial states, *i.e.* the difference between the bottom-induced and gluon-induced processes. We also see that for smaller values of  $m_b$  the Higgs distributions become slightly softer. While naively the finite phase space would move the  $p_{T,H}$  distributions to a softer regime when we increase the bottom mass, the opposite happens: a smaller bottom mass in the final state jet cuts off the  $p_{T,b}$  distributions at smaller values of  $p_{T,b}$ . Because for both bottom-exclusive processes the charged Higgs bosons balance the final state bottom jet in the transverse plane, the  $p_T$  spectrum for all particles becomes softer when the bottom jets become softer, which is the case for a smaller cutoff value  $p_{T,b}^{\min} \sim m_b$ . However, this effect is already part of the collinear bottom quark approximation, which we consider next. Therefore, at this point we conclude that bottom quark mass effects are negligible compared to the collinear bottom quark approximation.

**Collinear approximation:** From the above considerations we know that the dominant error is the assumption that the final state bottom jets are collinear and are resummed into the bottom parton densities. We can test the validity of this assumption using the NLO differential cross sections for the process  $b\bar{b} \rightarrow H^+H^-$ : part of the NLO corrections are real jet emission diagrams, either real gluon emission from the Born process or the bottom quark emission  $bg \rightarrow bH^+H^-$ , which we usually refer to as crossed diagrams. In Fig. 4 we saw (and discussed in detail) that, in the limit of  $\mu_F \rightarrow m_b$ , the perturbative expansion around the LO process  $b\bar{b} \rightarrow H^+H^-$  fails. The bottom parton density becomes small, because it is defined to include the splitting of the gluon into a bottom pair up to  $p_{T,b} < \mu_F$ . With the lower cutoff  $p_{T,b}^{\min} \sim m_b$  this means that less gluon splitting is included in the bottom parton density and more of it has to be considered explicitly, which in turn means accounting for the gluon-initiated process  $bg \rightarrow bH^+H^-$ , and eventually  $gg \rightarrow b\bar{b}H^+H^-$ . As we have seen, the  $K$  factor for the process  $b\bar{b} \rightarrow H^+H^-$  blows up in this limit, because already the NLO contribution  $bg \rightarrow bH^+H^-$  becomes dominant.

This behavior illustrates how the variation of  $\mu_F$  interpolates consistently between two regimes: for large  $\mu_F$  the LO process  $b\bar{b} \rightarrow H^+H^-$  is dominant. In fact, for  $\mu_{F,b} = m_H/2$  it is designed precisely to minimize the effect of the NLO contribution  $bg \rightarrow bH^+H^-$  [6, 26]. For smaller  $\mu_F$  the formerly NLO contribution  $bg \rightarrow bH^+H^-$  will become dominant. The NLO calculation of  $b\bar{b} \rightarrow H^+H^-$  combines these two processes consistently (using the zero bottom quark mass approximation,

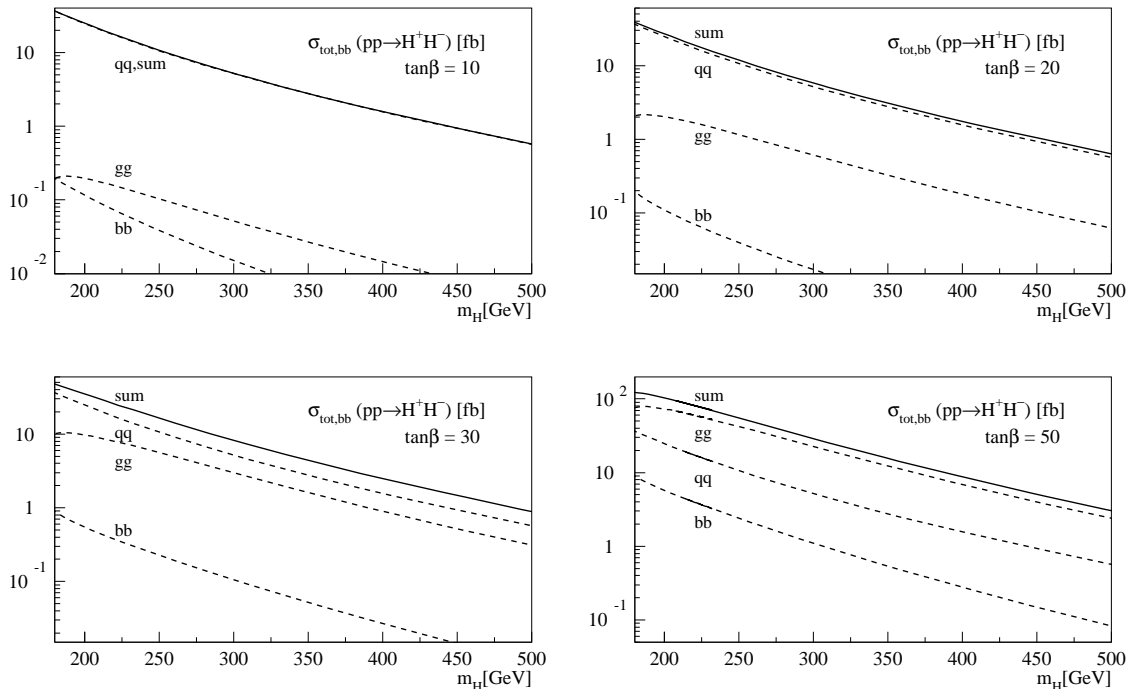


Figure 7: Production cross sections for pair production of charged Higgs bosons. The curves for the bottom-induced process (sum of  $s$ - and  $t$ -channel) is labeled  $bb$ . The Drell–Yan process with only light-flavor incoming quarks is labeled  $DY$ , and the gluon fusion process through the one-loop amplitude is labeled  $gg$ . The cross sections are given for different values of  $\tan\beta$ . The bottom-induced production rate and the Drell–Yan production rates are computed at NLO.

which we tested above) [6, 7]. We should note that a NNLO calculation including the  $gg \rightarrow b\bar{b}H^+H^-$  subprocess would of course be perfectly suited for this test, but goes beyond the scope of our paper. Moreover, we emphasize that if the bottom-parton approach using the collinear bottom quark approximation should not work well, this behavior will already show up in the NLO interpolation.

In Fig. 6 we show the numerical results of this comparison. As usual, we test the assumption for two values of  $\tan\beta$  or in other words independently for the  $s$ -channel and  $t$ -channel subprocesses. All shifts from LO to NLO curves were discussed in section II. To test the bottom-parton approximation we now change the factorization scale to  $\mu_F = 20$  GeV. We see that for both the  $s$ -channel and  $t$ -channel processes the  $p_T$  distributions become slightly harder when we compare the leading order and the low-scale curves. The now-dominant three particle kinematics is responsible for this shift. In an earlier work we showed that part of this effect is also due to the hardening gluon spectrum when we move to smaller values of  $\mu_F \equiv \mu_{F,g}$  in the bottom-gluon initial state [7]. We note, however, that the shifts in the  $p_{T,H}$  and  $y_H$  distributions are well within the perturbative uncertainty. As we discussed in section II, the NLO distributions for the central factorization scale  $\mu_F = m_H/2$  have to interpolate between the LO and the low-scale curves, because they are affected by the two- and three-particle kinematics. It is a curious coincidence that the NLO rapidity distributions for this scale choice are much more similar between the  $s$ - and  $t$  channels than any of the other cases. We therefore conclude that the collinear approximation in the bottom-parton picture is indeed valid for the distributions of the (heavy) final states. We have made similar checks for larger Higgs masses, and both the zero-mass and collinear approximations improve in accuracy. This is in agreement of what one would expect from the bottom-parton approach [28].

#### IV. COMBINATION OF PRODUCTION PROCESSES

Charged Higgs boson pairs can be produced in three different ways at the LHC [13]. Theoretically the most straight-forward production process is light-flavor quark scattering via an  $s$ -channel photon and  $Z$  [11]. As described in section II, the charged Higgs couplings are nearly independent of  $\tan\beta$ , as long as the pseudoscalar Higgs mass and the charged Higgs mass are large enough. We calculate the NLO production cross section in complete analogy to the production of two supersymmetric sleptons, a production process which is part of the publicly available computer program Prospino2 [30]. The factorization and

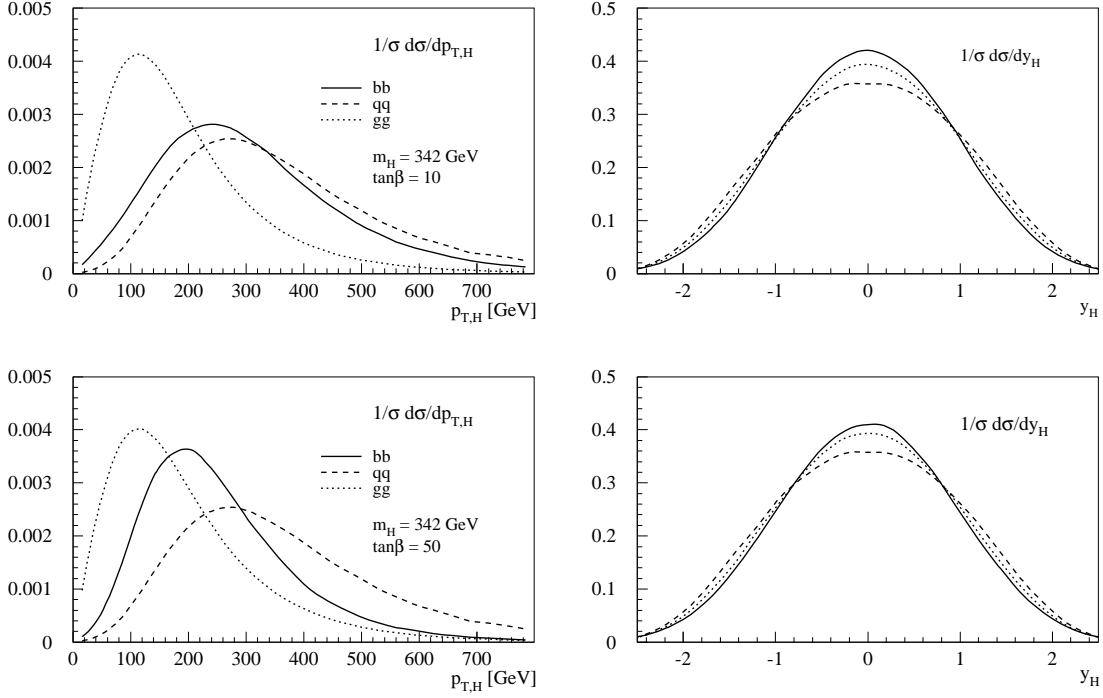


Figure 8: The rapidity and transverse momentum distributions of the final state charged Higgs boson for the three different production mechanisms. The curves for the bottom-induced process are labeled  $bb$ . The Drell-Yan process with only light-flavor incoming quarks is labeled  $qq$ , and the gluon fusion process through the one-loop amplitude is labeled  $gg$ . The bottom-induced production rate and the Drell-Yan production rates are computed at NLO.

renormalization scales are chosen as  $m_H$ . In Fig. 7 we see that for charged Higgs masses between 160 and 500 GeV the NLO rate Drell-Yan process varies between 58 fb and 0.23 fb. This rate is computed without any cuts on the final state particles. The size of the NLO corrections for this process varies from  $K = 1.27$  to  $K = 1.17$  (for Higgs masses from 160 GeV to 500 GeV). The remaining theoretical error on the NLO cross section can be estimated to be less than 25% [30]. For small values of  $\tan\beta \lesssim 20$  this production process is the dominant channel at the LHC.

Similar to the light-flavor Drell-Yan process, charged Higgs pairs can also be produced in bottom-parton scattering. We analyzed this production process in detail in this paper and can now quote a reliable estimate of the production cross section. We find that the  $s$ -channel and the  $t$ -channel subprocesses interfere destructively. The LO total cross section is enhanced by  $\tan^4\beta$  for large values of  $\tan\beta$ . In Fig. 7 we see that even for  $\tan\beta = 50$  the NLO cross section is still below 10 fb. In this region of parameter space the  $t$ -channel subprocess dominates completely. Compared to earlier analyses we find that we have to use running  $\overline{\text{MS}}$  Yukawa couplings and a low bottom factorization scale, which suppresses the cross section to a level where it will always stay below the light-flavor induced rate as well as below the gluon-induced process discussed in the next paragraph. The remaining theoretical error on this total cross section we estimated in section II to be on the order of 25%.

For large values of  $\tan\beta$ , the one-loop process  $gg \rightarrow H^+H^-$  cross section also increases like  $\tan^4\beta$ . In the 2HDM this process proceeds through a mixed top-bottom loop or through an  $s$ -channel neutral Higgs boson. Even though our estimate of the gluon fusion rate is less precise than for the other two channels, we use our LO estimate to compare the power of the different channels. The theoretical uncertainty we would attach to this LO cross section prediction is probably around a factor of two. However, we believe that quoting the LO rate is conservative: we expect the NLO corrections to be dominated by initial-state radiation and therefore similar to the neutral Higgs pair production counterpart [36]. As is seen in numerous processes, this universal initial state radiation leads to large positive corrections. We also note that this process is not evaluated with  $\overline{\text{MS}}$  Yukawa couplings, but with their on-shell definition. For loop-induced processes of this type, this renormalization scheme leads to a well-behaved perturbative series [37]. The gluon fusion rate has a minimum around  $\tan\beta = 7$ , and in Fig. 7 we see that it passes the (constant) Drell-Yan process at the LHC for  $\tan\beta \gtrsim 40$ . As stated before, the bottom-parton scattering rate is always smaller than the loop-induced gluon fusion rate for production of charged Higgs boson pairs at the LHC.

Naïvely adding the rates for the three production mechanisms for charged Higgs boson pair production is consistent, and it tells us which process contributes what fraction of the events to the total cross section. However, it will not be the entire story. Detector analyses require acceptance cuts on the Higgs decay products, and these cuts will also probe the distributions of

mSUGRA	$m_H$	$\tan \beta$	$m_0$	$m_{1/2}$	$A_0$	$m_{\tilde{g}}$	$\mu$	$\sigma_{\text{LO}}[\text{fb}]$	$\sigma_{\text{NLO}}[\text{fb}]$	$\Delta_b$	non- $\Delta_b$
1a	409	10	100	250	-100	608	358	$1.6 \times 10^{-3}$	$2.8 \times 10^{-3}$	-19%	0.8%
1b	534	30	200	400	0	938	516	$4.1 \times 10^{-3}$	$5.5 \times 10^{-3}$	-40%	2.7%
2	1519	10	1450	300	0	782	483	$8.0 \times 10^{-8}$	$2.3 \times 10^{-7}$	-8.2%	3.1%
3	595	10	90	400	0	935	524	$1.6 \times 10^{-4}$	$2.9 \times 10^{-4}$	-19%	0.6%
4	342	50	400	300	0	733	396	$5.3 \times 10^{-1}$	$6.0 \times 10^{-1}$	-54%	3.9%
5	698	5	150	300	-1000	724	638	$1.1 \times 10^{-4}$	$1.9 \times 10^{-4}$	-17%	1.1%
GMSB			$\Lambda$	$M_{\text{mes}}$	$N_{\text{mes}}$						
7	398	15	$40 \times 10^3$	$80 \times 10^3$	3	946	310	$1.2 \times 10^{-3}$	$2.5 \times 10^{-3}$	-13%	0.1%
8	543	15	$100 \times 10^3$	$200 \times 10^3$	1	835	423	$2.0 \times 10^{-4}$	$4.0 \times 10^{-4}$	-13%	0.2%
AMSB			$m_0$	$m_{\tilde{G}}$							
9	1050	10	400	$60 \times 10^3$		1283	1022	$2.5 \times 10^{-6}$	$5.4 \times 10^{-6}$	-25%	1.6%

Table I: Supersymmetric corrections to the production cross section  $b\bar{b} \rightarrow H^+H^-$  from the resummed  $\Delta_b$  corrections and explicit remaining supersymmetric loop diagrams. The supersymmetric parameter points are chosen according to the benchmarks in Ref. [35]. All masses are given in units of GeV. The percentage changes are defined with respect to 2HDM rates at NLO.

the charged Higgs bosons. Therefore, we have to compare the transverse momentum and rapidity distributions of the charged Higgs bosons in the three different production mechanisms. As before, we use the NLO results for the bottom-parton scattering process and the Drell-Yan process. The comparison is shown in Fig. 8. As usual, we show the results for two different values of  $\tan \beta$ , which distinguish the  $s$ -channel ( $\tan \beta = 10$ ) and the  $t$ -channel ( $\tan \beta = 50$ ) contributions. In contrast to bottom-parton scattering, we see that the distributions for the Drell-Yan and gluon fusion processes do not depend on  $\tan \beta$ . For Drell-Yan  $s$ -channel photon and  $Z$  exchange this reflects the fact that the entire scattering matrix element is to a good approximation independent of  $\tan \beta$  (for large enough  $m_H$ ). In gluon fusion, the steep  $x$  behavior of the gluon parton distributions pushes the produced heavy particles close to threshold, which means the two charged Higgs bosons appear with very little transverse momentum. Again, this feature is independent of  $\tan \beta$ . The bottom-parton scattering spectrum varies strongly with the relative weight of the  $s$ -channel and the  $t$ -channel diagrams. At threshold,  $t$ -channel top quark exchange ( $S$ -wave) increases rapidly with  $\beta$ , much faster than  $s$ -channel gauge boson exchange ( $P$ -wave), which shows a delayed increase, as  $\beta^3$ . The transverse momentum spectrum becomes softer the more the  $t$ -channel contributes, *i.e.* for larger values of  $\tan \beta$ . This effect is particularly strong because the bottom parton densities are derived from the gluon density and therefore are steep in  $x$ , pushing the partonic center-of-mass energy to the smallest possible values.

## V. SUPERSYMMETRIC CONTRIBUTION TO BOTTOM-INDUCED PROCESS

Diagrams with a gluino instead of a gluon contribute to the NLO rate for the process  $pp \rightarrow H^+H^-$ . However, for massive gluinos only virtual diagrams appear, in which the gluon and the quark lines are replaced by gluinos and squarks. Usually, the SUSY contributions are suppressed by the large supersymmetric partner masses. However, there is a well-known exception to this rule, where the power suppression by large sbottom masses can be compensated by the gluino mass and the Higgsino mass parameter in the numerator. Sbottom-gluino corrections to the external (massless) bottom legs can involve a left-right mixing for the sbottom propagator. Because the off-diagonal matrix element in the sbottom mass matrix has the form  $m_b(A_b - \mu \tan \beta)$  the left-right mixing is enhanced by a factor  $\tan \beta$ . These potentially large corrections will automatically become important for charged Higgs searches whenever we rely on a large production rate with values  $\tan \beta \gtrsim 30$  in an MSSM framework. However, we also note that these corrections introduce a huge new set of parameters into charged Higgs searches, where it is not even clear if charged Higgs searches at the LHC should be part of the search for supersymmetry or something more general. We leave it to the reader to decide this issue, and present the size of the additional supersymmetric corrections in this section.

Just like in mass renormalization, the supersymmetric external bubbles can be resummed. It has been shown that this resummation consistently takes into account the leading contributions in  $\tan \beta$  [38]. Note that in the large  $\tan \beta$  limit we approximate the off-diagonal matrix element as  $-m_b \mu \tan \beta$  and it is an unsolved problem how to treat the  $m_b A_b$  term consistently. We will not resum this contribution. The difference is in any case numerically small, because we are interested only in the region of parameter space where  $\tan \beta$  is large enough to also ensure  $\mu \tan \beta \gg A_b$ . If we start from the fixed relation between the bottom quark mass and the bottom Yukawa coupling (which we of course break in our calculation with a vanishing bottom mass and a running  $\overline{\text{MS}}$  bottom Yukawa coupling) we can regard the resummed bottom self-energy diagrams as a shift in the Yukawa coupling as compared to the mass or its fixed order value:

$$\begin{aligned}
\frac{m_b \tan \beta}{v} &\rightarrow \frac{m_b \tan \beta}{v} \frac{1}{1 + \Delta_b} \\
\Delta_b &= \frac{\sin(2\theta_b)}{m_b} \frac{\alpha_s}{4\pi} C_F m_{\tilde{g}} \frac{1}{i\pi^2} \left[ B(0, m_{\tilde{b},2}, m_{\tilde{g}}) - B(0, m_{\tilde{b},1}, m_{\tilde{g}}) \right] \\
&= \frac{\alpha_s}{2\pi} C_F m_{\tilde{g}} (-A_b + \mu \tan \beta) I(m_{\tilde{b},1}, m_{\tilde{b},2}, m_{\tilde{g}}) \\
I(a, b, c) &= -\frac{1}{(a^2 - b^2)(b^2 - c^2)(c^2 - a^2)} \left[ a^2 b^2 \log \frac{a^2}{b^2} + b^2 c^2 \log \frac{b^2}{c^2} + c^2 a^2 \log \frac{c^2}{a^2} \right]. \tag{1}
\end{aligned}$$

The function  $B(p^2, m_1, m_2)$  is the usual scalar two-point function;  $C_F = 4/3$  is the Casimir factor in the fundamental representation of  $SU(3)$ . As mentioned above, there are similar additional terms proportional to the strong coupling or to the top quark Yukawa coupling, but the  $\Delta_b$  correction is the leading contribution for large  $\tan \beta$ . We should also note that the resummed definition of these corrections is well defined for all  $\Delta_b > -1$ , whereas the strictly fixed order series which yields  $(1 - 4\Delta_b)$  breaks down for  $\Delta_b > 1/4$ .

We show the numerical results for the supersymmetric corrections to the total rate in Tab. I. To illustrate the effect of the supersymmetric corrections we follow the SPS parameter points, which are obviously not designed to advertise searches for charged Higgs pairs in bottom-parton scattering. Apart from the fact that almost all 2HDM production cross sections are very small, we indeed see that the  $\Delta_b$  corrections are by far dominant, and that the remaining explicit diagrams contribute at a level well below the total cross section theoretical uncertainty. The fact that all  $\Delta_b$  corrections are negative reflects the fact that all SPS points are chosen with  $\mu > 0$ , a preference triggered by indirect constraints, such as measurements of the muon anomalous magnetic moment ( $g_\mu - 2$ ) or the rare decay  $b \rightarrow s\gamma$ .

Of course, all of the processes evaluated in section IV receive explicit supersymmetric corrections. For the Drell–Yan process we know that their effects are small [30], because there are no couplings enhanced by  $\tan \beta$ . For gluon fusion, the effects of squark loops can be very large if the squarks are light. We do not include these additional diagrams in this paper, because they require a careful analysis of the MSSM parameter space. Instead, we refer the reader to dedicated studies in Refs. [13, 14]. We should also mention that fairly light charged Higgs bosons in an MSSM framework can be visible in cascade decays of heavy squarks and gluinos [39]. Because the production rates of squarks and gluinos are of the order of  $\mathcal{O}(10 \text{ pb})$  at the LHC, even a small branching fraction to charged Higgs bosons can be very promising.

## VI. CONCLUSIONS

To obtain a reliable prediction for the rate of charged Higgs boson pair production at the LHC we have computed the process  $b\bar{b} \rightarrow H^+H^-$  to NLO. In previous studies [13], the bottom-parton scattering process had been the source of large theoretical uncertainty. With our improved understanding of bottom parton densities [6, 7, 26], we now have a recipe for calculating processes involving initial-state bottom quarks. To test the perturbative behavior of the LO prediction for  $b\bar{b} \rightarrow H^+H^-$ , we study NLO corrections to the total rate as well as to the kinematical distributions of the heavy final state Higgs bosons. Moreover, we use the NLO calculation to carefully verify the validity of the bottom-parton approach.

With this reliable prediction for the total cross section of the bottom-induced production process at hand, we compare its rate to Drell–Yan pair production via an  $s$ -channel gauge boson. This process is available at NLO through Prospino2 [30]. The third production mechanism which we include in the comparison is the gluon-fusion process with a one-loop amplitude including a mixed top-bottom loop [12]. Like the bottom-parton scattering process its rate grows like  $\tan^4 \beta$  for large values of  $\tan \beta$ . We find that for low values of  $\tan \beta$  the Drell–Yan process is by far dominant, and that for large values of  $\tan \beta$  the loop-induced process overwhelms the other two. Bottom-induced production will gain relative importance only if supersymmetric loop contributions reduce the rate of the top-bottom loop [13, 14], or if the bottom-parton induced rate is enhanced by universal supersymmetric corrections to the bottom Yukawa coupling. Finally, we show how a combined sample of charged Higgs pair events would look at the LHC, including the distinctly different transverse momentum spectra of the three different production processes.

Note added: While we were in the process of finalizing this work, another paper [40] appeared in which the authors present results which correspond to parts of our sections II and V.

### Acknowledgments

We would like to thank Oscar Éboli for many enlightening discussions and for his technical help. Moreover, TP would like to thank Oscar Éboli and the University of São Paulo for their hospitality while large fractions of the results presented in this paper were calculated. Last, but not least we are very grateful to David Rainwater and Oscar Éboli for their critical review of the manuscript. This work was supported in part by Fundação de Amparo à Pesquisa do Estado de São Paulo (FAPESP) through grant 04/01183-2 (AA).

- 
- [1] D. Abbaneo *et al.* [LEPEWWG], arXiv:hep-ex/0212036.
- [2] T. Plehn, D. Rainwater and D. Zeppenfeld, Phys. Lett. B **454**, 297 (1999); T. Plehn, D. L. Rainwater and D. Zeppenfeld, Phys. Rev. D **61**, 093005 (2000); M. Schumacher, arXiv:hep-ph/0410112.
- [3] E. Boos, A. Djouadi and A. Nikitenko, Phys. Lett. B **578**, 384 (2004).
- [4] see *e.g.* G. F. Giudice, R. Rattazzi and J. D. Wells, Nucl. Phys. B **595**, 250 (2001); U. Mahanta and S. Rakshit, Phys. Lett. B **480**, 176 (2000); U. Mahanta and A. Datta, Phys. Lett. B **483**, 196 (2000); C. Csaki, M. L. Graesser and G. D. Kribs, Phys. Rev. D **63**, 065002 (2001); K. m. Cheung, Phys. Rev. D **63**, 056007 (2001).
- [5] R. M. Barnett, H. E. Haber and D. E. Soper, Nucl. Phys. B **306**, 697 (1988); A. C. Bawa, C. S. Kim and A. D. Martin, Z. Phys. C **47**, 75 (1990); V. D. Barger, R. J. Phillips and D. P. Roy, Phys. Lett. B **324**, 236 (1994) S. Moretti and K. Odagiri, Phys. Rev. D **55**, 5627 (1997); F. Borzumati, J. L. Kneur and N. Polonsky, Phys. Rev. D **60**, 115011 (1999).
- [6] T. Plehn, Phys. Rev. D **67**, 014018 (2003).
- [7] E. L. Berger, T. Han, J. Jiang and T. Plehn, arXiv:hep-ph/0312286.
- [8] S. H. Zhu, Phys. Rev. D **67**, 075006 (2003); J. Alwall and J. Rathsmann, JHEP **0412**, 050 (2004); N. Kidonakis, arXiv:hep-ph/0412422.
- [9] D. A. Dicus, J. L. Hewett, C. Kao and T. G. Rizzo, Phys. Rev. D **40**, 787 (1989); A. A. Barrientos Bendezu and B. A. Kniehl, Phys. Rev. D **59**, 015009 (1999); and Phys. Rev. D **63**, 015009 (2001); O. Brein, W. Hollik and S. Kanemura, Phys. Rev. D **63**, 095001 (2001); Z. Fei, M. Wen-Gan, J. Yi, H. Liang and W. Lang-Hui, Phys. Rev. D **63**, 015002 (2001).
- [10] W. Hollik and S. H. Zhu, Phys. Rev. D **65**, 075015 (2002).
- [11] E. Eichten, I. Hinchliffe, K. D. Lane and C. Quigg, Rev. Mod. Phys. **56**, 579 (1984) [Addendum-ibid. **58**, 1065 (1986)]; N. G. Deshpande, X. Tata and D. A. Dicus, Phys. Rev. D **29**, 1527 (1984).
- [12] S. S. D. Willenbrock, Phys. Rev. D **35**, 173 (1987); A. Krause, T. Plehn, M. Spira and P. M. Zerwas, Nucl. Phys. B **519**, 85 (1998);
- [13] A. A. Barrientos Bendezu and B. A. Kniehl, Nucl. Phys. B **568**, 305 (2000).
- [14] O. Brein and W. Hollik, Eur. Phys. J. C **13**, 175 (2000).
- [15] J. F. Gunion, H. E. Haber, F. E. Paige, W. K. Tung and S. S. Willenbrock, Nucl. Phys. B **294**, 621 (1987).
- [16] D. A. Dicus, K. J. Kallianpur and S. S. D. Willenbrock, Phys. Lett. B **200**, 187 (1988); S. Moretti, J. Phys. G **28**, 2567 (2002).
- [17] S. Moretti and J. Rathsmann, Eur. Phys. J. C **33**, 41 (2004).
- [18] D. P. Roy, Phys. Lett. B **459**, 607 (1999); E. Christova, H. Eberl, W. Majerotto and S. Kraml, JHEP **0212**, 021 (2002).
- [19] K. A. Assamagan and Y. Coadou, Acta Phys. Polon. B **33**, 707 (2002); Y. Coadou, FERMILAB-THESIS-2003-31.
- [20] R. Kinnunen and A. Nikitenko, report CMS note 2003/006.
- [21] J. F. Gunion, Phys. Lett. B **322**, 125 (1994); J. A. Coarasa, D. Garcia, J. Guasch, R. A. Jimenez and J. Sola, Phys. Lett. B **425**, 329 (1998); S. Moretti and D. P. Roy, Phys. Lett. B **470**, 209 (1999).
- [22] K. A. Assamagan, Y. Coadou and A. Deandrea, report ATL-COM-PHYS-2002-002, arXiv:hep-ph/0203121; K. A. Assamagan and N. Gollub, arXiv:hep-ph/0406013.
- [23] P. Salmi, R. Kinnunen and N. Stepanov, arXiv:hep-ph/0301166.
- [24] K. A. Assamagan, Acta Phys. Polon. B **31**, 881 (2000); S. Moretti, Phys. Lett. B **481**, 49 (2000)
- [25] J. C. Collins and W. K. Tung, Nucl. Phys. B **278**, 934 (1986); M. A. Aivazis, J. C. Collins, F. I. Olness and W. K. Tung, Phys. Rev. D **50**, 3102 (1994); F. I. Olness and W. K. Tung, Nucl. Phys. B **308**, 813 (1988); M. Krämer, F. I. Olness and D. E. Soper, Phys. Rev. D **62**, 096007 (2000).
- [26] E. Boos and T. Plehn, Phys. Rev. D **69**, 094005 (2004).
- [27] R. V. Harlander and W. B. Kilgore, Phys. Rev. D **68**, 013001 (2003).
- [28] F. Maltoni, Z. Sullivan and S. Willenbrock, Phys. Rev. D **67**, 093005 (2003); H. S. Hou, W. G. Ma, R. Y. Zhang, Y. B. Sun and P. Wu, JHEP **0309**, 074 (2003); S. Dawson, C. B. Jackson, L. Reina and D. Wackerroth, arXiv:hep-ph/0408077.
- [29] S. Dittmaier, M. Kramer and M. Spira, Phys. Rev. D **70**, 074010 (2004); S. Dawson, C. B. Jackson, L. Reina and D. Wackerroth, Phys. Rev. D **69**, 074027 (2004).
- [30] W. Beenakker, R. Höpker, M. Spira and P. M. Zerwas, Nucl. Phys. B **492**, 51 (1997); W. Beenakker, M. Klasen, M. Krämer, T. Plehn, M. Spira and P. M. Zerwas, Phys. Rev. Lett. **83**, 3780 (1999); W. Beenakker, M. Krämer, T. Plehn, M. Spira and P. M. Zerwas, Nucl. Phys. B **515**, 3 (1998); Prospino2.0, <http://pheno.physics.wisc.edu/~plehn>
- [31] J. Pumplin, D. R. Stump, J. Huston, H. L. Lai, P. Nadolsky and W. K. Tung, JHEP **0207**, 012 (2002)
- [32] for a review see *e.g.* B. W. Harris and J. F. Owens, Phys. Rev. D **65**, 094032 (2002).
- [33] see *e.g.* M. Carena, J. R. Espinosa, M. Quiros and C. E. M. Wagner, Phys. Lett. B **355**, 209 (1995); G. Degrossi, S. Heinemeyer, W. Hollik, P. Slavich and G. Weiglein, Eur. Phys. J. C **28**, 133 (2003); S. Heinemeyer, W. Hollik and G. Weiglein, arXiv:hep-ph/0412214.
- [34] A. Alves, O. Éboli and T. Plehn, Phys. Lett. B **558**, 165 (2003).

- [35] B. C. Allanach *et al.*, in *Proc. of the APS/DPF/DPB Summer Study on the Future of Particle Physics (Snowmass 2001)* ed. N. Graf, Eur. Phys. J. C **25**, 113 (2002); N. Ghobane and H. U. Martyn, in *Proc. of the APS/DPF/DPB Summer Study on the Future of Particle Physics (Snowmass 2001)* ed. N. Graf, arXiv:hep-ph/0201233.
- [36] E. W. N. Glover and J. J. van der Bij, Nucl. Phys. B **309**, 282 (1988); T. Plehn, M. Spira and P. M. Zerwas, Nucl. Phys. B **479**, 46 (1996) [Erratum-ibid. B **531**, 655 (1998)]; S. Dawson, S. Dittmaier and M. Spira, Phys. Rev. D **58**, 115012 (1998).
- [37] M. Spira, Fortsch. Phys. **46**, 203 (1998).
- [38] L. J. Hall, R. Rattazzi and U. Sarid, Phys. Rev. D **50**, 7048 (1994); M. Carena, M. Olechowski, S. Pokorski and C. E. Wagner, Nucl. Phys. B **426**, 269 (1994); M. Carena, D. Garcia, U. Nierste and C. E. Wagner, Nucl. Phys. B **577**, 88 (2000); A. Belyaev, D. Garcia, J. Guasch and J. Sola, Phys. Rev. D **65**, 031701 (2002) [arXiv:hep-ph/0105053]; J. Guasch, P. Häfliger and M. Spira, arXiv:hep-ph/0305101.
- [39] A. Datta, A. Djouadi, M. Guchait and Y. Mambrini, Phys. Rev. D **65**, 015007 (2002);
- [40] H. Hong-Sheng, M. Wen-Gan, Z. Ren-You, J. Yi, H. Liang and X. Li-Rong, arXiv:hep-ph/0502214.
- [41] Note that this  $\beta$  has nothing to do with  $\tan \beta$ , it is defined as  $\beta = \sqrt{1 - 4m_H^2/\hat{s}}$ . Since both definitions are very common and there is little chance to confuse them we prefer to stick to this notation.